FINAL REPORT

submitted to

National Aeronautics and Space Administration
Lyndon B. Johnson Space Center
Space Science Branch, Code SN3
ATTN: Eric L. Christiansen
Houston, TX 77058

for research entitled

# SIMULATION OF HYPERVELOCITY IMPACT ON ALUMINUM-NEXTEL-KEVLAR ORBITAL DEBRIS SHIELDS

## (NCC 9-73)

submitted by

Eric P. Fahrenthold
Department of Mechanical Engineering
University of Texas
Austin, TX 78712

June 30, 2000

## ABSTRACT

An improved hybrid particle-finite element method has been developed for hypervelocity impact simulation. The method combines the general contact-impact capabilities of particle codes with the true Lagrangian kinematics of large strain finite element formulations. Unlike some alternative schemes which couple Lagrangian finite element models with smooth particle hydrodynamics, the present formulation makes no use of slidelines or penalty forces. The method has been implemented in a parallel, three dimensional computer code.

Simulations of three dimensional orbital debris impact problems, using this parallel hybrid particle-finite element code, show good agreement with experiment and good speedup in parallel computation. The simulations included single and multi-plate shields as well as aluminum and composite shielding materials, at an impact velocity of eleven kilometers per second.

# 1 Introduction

The orbital debris hazard to the International Space Station (ISS) and other space structures has focused a significant research effort on the problem of spacecraft shielding design. To date shield design work has relied primarily on experimental hypervelocity impact research (Christiansen et al., 1999), with impact simulation playing a relatively minor role. However a number of factors suggest that future design work will place increased emphasis on the use of simulation:

- Experimental studies using light gas guns (LGG) and inhibited shaped charge launchers (ISCL) are at present unable to investigate the entire projectile velocity and kinetic energy range of interest
- The increased use of composite materials (in both shielding and aerospace structures) and the introduction of multi-layered shields has greatly expanded the number of experiments required to fully investigate each shielding design problem
- An emphasis on faster, lower cost design methods in a maturing aerospace industry motivates the expanded use of computer aided design tools
- The increased availability of high performance and massively parallel computing hardware will expand the range of design problems which can be investigated through simulation

Despite these strong motivations, progress in the application of impact codes to spacecraft shielding design problems has been relatively slow. The most important reason is that the numerical methods embodied in traditional continuum Lagrangian and Eulerian codes are not well suited to address certain noncontinuum physics associated with the shielding design problem (Fahrenthold, 1998). Hence initial work on the application of conventional continuum codes to debris shield impact simulations has been followed by a period of research,

during which alternative numerical methods have been tested, modified, and/or developed to better address the problem of interest.

Most recent work simulating orbital debris impact effects has employed either pure particle or mixed particle-continuum methods (Hayhurst et al., 1998 and Fahrenthold and Horban, 1999) since only particle-based kinematic schemes offer both an efficient solution to the debris propagation problem and an entirely general representation of contact-impact. Work based on pure particle methods has encountered difficulties with accurate modeling of material strength effects (Faraud et al., 1999), and other complications (Libersky et al., 1997). It appears that some mixed or hybrid particle-continuum method will prove most effective in meeting the need for fundamental improvements in simulation-based design of orbital debris shielding.

The present report describes work performed to evaluate a particular new hybrid particle-continuum method (Fahrenthold and Horban, 2000), developed to simulate orbital debris impact problems. The numerical method is evaluated here, via simulation of a set of ISCL experiments, the latter conducted by Grosch (1996 and 1997) to investigate the performance of ISS shielding in oblique impacts at a velocity of eleven kilometers per second. The simulations discussed include: (1) both Whipple and multi-plate shield designs, (2) both aluminum and composite shielding materials, and (3) both hollow cylindrical projectiles (produced by the ISC launchers) and mass equivalent spherical projectiles (for comparison to lower velocity LGG tests).

The simulations were performed using a parallel code written by the author. In addition to the simulation results, speedup data is presented for test problems run on up to 128 processors, on an Origin 2000 system operated by the Numerical Aerospace Simulation facility at NASA Ames Research Center.

## 2 Numerical method

A detailed description of the hybrid particle-finite element technique used here is provided in later sections. A brief summary of the numerical method follows.

In the hybrid formulation employed here, particles and finite elements are used simultaneously but not redundantly to represent different physical effects. The particles are used to represent all inertia effects as well as the thermomechanical response of the medium in compressed states. The particle center of mass coordinates in the reference configuration define Lagrangian finite elements, which are simultaneously employed to represent interparticle forces associated with tension and elastic-plastic shear. Damage variables are introduced as internal states for the finite elements, and evolve with the material history to represent the loss of tensile and shear strength and stiffness under thermomechanical loading. Element failure due to spall, melting, accumulated plastic strain or other physical criteria results in the loss of interparticle forces associated with element shear and tension, so that particles unassociated with any intact elements are free to flow under contact-impact loads. No mass or energy is discarded at element failure, and no rezoning is required to model the transition from an intact to a fragmented medium.

This hybrid modeling technique avoids the tensile instabilities and numerical fracture problems which arise with some pure particle methods, the use of slidelines and penalty forces which characterize pure Lagrangian finite element methods, and the mixed material thermodynamics and numerical diffusion which are features of Eulerian techniques. As indicated in the sections which follow, this hybrid particle-element methodology can be effectively applied in the simulation of rather complex three dimensional debris shielding problems.

## 3 Hypervelocity impact simulation

Most computer simulation work on hypervelocity impact problems has employed either Lagrangian finite element techniques (Hallquist, 1983) or Eulerian finite difference or finite volume techniques (McGlaun et al., 1990). The advantages and disadvantages of such methods are well known, and have led to the application of different codes to distinct problem classes. Recent numerical methods research (Belytschko et al., 1996 and Liu et al.. 2000) has included a focus on the development of new Arbitrary Lagrangian-Eulerian (ALE. Budge and Peery, 1993), smooth particle hydrodynamic (SPH, Stellingwerf and Wingate, 1993), and mixed particle-continuum methods (Hayhust et al., 1998 and Fahrenthold. 1998) for problems which are difficult to address with traditional Lagrangian or Eulerian techniques. An example of the latter class of problems is the simulation of hypervelocity impact on orbital debris shielding (Christiansen et al., 1999).

Although significant advances have been made in the formulation and improvement of ALE and SPH techniques, it appears from work to date (Libersky et al.. 1997 and Faraud et al., 1999) that some mixed particle-continuum formulation is best suited to address the orbital debris shielding problem. The most popular type of mixed-particle continuum approach is a *coupled* SPH-finite element formulation. The latter approach has been implemented in the EPIC (Johnson et al., 1993), and AUTODYN (Hayhust et al., 1998) codes, and in general relies on a penalty-based contact-impact algorithm to link conventional SPH and Lagrangian finite element models. An alternative mixed particle-continuum formulation was developed by Fahrenthold and Horban (1999). The latter approach may be characterized as a *hybrid* (as opposed to a *coupled*) formulation, since it makes simultaneous use of both elements and particles to model distinct physical effects in all of the impacting materials.

The hybrid particle-element formulation of Fahrenthold and Horban (1999) employed deforming Lagrangian particles and a penalty method to represent contact-impact. In the interest of eliminating the penalty treatment of contact-impact effects, Fahrenthold and Koo

(2000) modified the formulation, introducing a new kernel based density interpolation for compressed states, while retaining an element-based description of tension and shear. They demonstrated the effectiveness of this improved hybrid scheme in one dimensional thermoelastic shock compression and tensile wave propagation problems. The latter formulation was extended to the thermoelastic-plastic-damage case by Fahrenthold and Horban (2000). The present report outlines the last cited improved hybrid particle-element formulation, introduces new damage models and a rate dependent yield stress, and evaluates the formulation by comparing simulations to published results of hypervelocity impact experiments.

The principal advantage of the numerical method described here is its seamless integration of the general contact-impact capabilities of particle methods with the true Lagrangian strength models of finite element formulations. Its principal disadvantage is the computational cost of incorporating both element and particle kinematics in a single code, although it should be emphasized that nowhere are the particle based and element based computations redundant.

## 4 Modeling methodology

Development of the model described here is based on interpolation concepts derived from the particle and finite element literature and a Hamiltonian model formulation approach. A Hamiltonian methodology replaces the weighted residual solution techniques commonly applied in finite element analysis and a variety of (sometimes ad hoc) model formulation procedures used in pure particle based modeling. Total entropy variables are introduced here as Hamiltonian displacements, so that general thermomechanical dynamics are included in the formulation.

The fixed mass particles used in the present work are non-deforming, and are associated with kernel functions used to calculate the continuum density in compressed states. Associated with the mass of the ith particle ($m^{(i)}$) is a total entropy ($S^{(i)}$), so that mass density ($\rho^{(i)}$) and entropy per unit mass ($s^{(i)}$) are the thermodynamic states used to calculate the

particle pressures and temperatures for any chosen equations of state.

Here the particle center of mass coordinates ($\mathbf{c}^{(i)}$) in the reference configuration define connectivity's for large strain Lagrangian finite elements, with reference volumes $V_0^{(j)}$. In the reference configuration the particle packing scheme is body centered cubic, with eight corner particles defining a hexahedral finite element, the latter used to describe elastic ($\mathbf{E}^{e(j)}$) and plastic ($\mathbf{E}^{p(j)}$) strain tensors and thereby quantify elastic-plastic shearing deformation in the continuum. Associating the body centered particle in each element with each of the six faces of the aforementioned hexahedron defines six five-noded subelements whose reference volumes ($V_o^{(j,k)}$) and Jacobians ($J^{(j,k)}$) are used to quantify hydrostatic tension.

Normal ($D^{(j)}$) and deviatoric ($d^{(j)}$) continuum damage variables are introduced here for the finite elements, and are used to quantify reductions in element strength and stiffness, as a function of each element's thermal and mechanical loading history. The damage variables evolve from an initial (undamaged) value of zero, to a maximum value of one, the latter representing a complete loss of element cohesion. All strain energy release associated with damage evolution is accounted for, as irreversible entropy production, and no rezoning or mass discard is associated with element failure. Particles unassociated with any intact elements are free to flow in response to contact-impact loads.

The preceding methodology offers a unique combination of features, and is well suited to address particular hypervelocity impact applications. The sections which follow discuss the particle and element based interpolations, the stored energy functions for the modeled system, the dissipative process models, the entropy evolution relations, the final form of Hamilton's equations, and numerical application of the method.

## 5 Interpolations

The density interpolation for compressed states is

$$\rho^{(i)} = \rho_o^{(i)} + \hat{\rho}^{(i)} + \tilde{\rho}^{(i)} \tag{1}$$

where $\rho_o^{(i)}$ is the reference density for the ith particle and

$$\hat{\rho}^{(i)} = \sum_{j=1}^{\hat{n}^{(i)}} \rho_o^{(j)} \hat{W}^{(i,j)}, \qquad \tilde{\rho}^{(i)} = \sum_{j=1}^{\tilde{n}^{(i)}} \rho_o^{(j)} \tilde{W}^{(i,j)} \tag{2}$$

with $\hat{W}^{(i,j)}$ and $\tilde{W}^{(i,j)}$ kernel functions for reference configuration nearest neighbors and all other neighbor particles respectively. For a system of $n$ particles the summation limits satisfy

$$n = 1 + \hat{n}^{(i)} + \tilde{n}^{(i)} \tag{3}$$

Since the kernel functions are positive, the density calculated from the assumed interpolation has a lower bound $\rho_o^{(i)}$. The kernel functions assumed here are

$$\hat{W}^{(i,j)} = \frac{1}{\hat{n}^{(i)}} \sum_{j=1}^{\hat{n}^{(i)}} \{ [\frac{h_p^{(i)} + h_p^{(j)}}{r_{ij}}]^3 - 1 \} \, \Lambda(h_p^{(i)} + h_p^{(j)} - r_{ij}) \tag{4}$$

and

$$\tilde{W}^{(i,j)} = \frac{1}{2\alpha^3} \sum_{j=1}^{\tilde{n}^{(i)}} \{ [1 - \frac{r_{ij}}{2\, h_p^{(j)}}] \} \, \Lambda(2\, h_p^{(j)} - r_{ij}) \tag{5}$$

where $h_p^{(j)}$ is the effective radius of the ith particle, $r_{ij}$ is the particle separation distance, $\Lambda$ denotes the unit step function, and $\alpha$ is a constant which allows for close packing of the particles at the reference bulk density.

The hexahedral elements employed here are described elsewhere (e.g. Hallquist, 1983), so their interpolation is not discussed, except to note that hourglass deformation modes are avoided, via: (1) the use of subelement volumes to calculate hydrostatic tension, and (2) the use of a kernel based density function to describe compressed states.

## 6 Kinetic and internal energy

The Hamiltonian for the modeled system ($H$) is the sum of the kinetic ($T$) and internal ($U$) energy functions

$$H = T + U \tag{6}$$

The kinetic energy is

$$T = \sum_{i=1}^{n} \frac{1}{2} m^{(i)-1} \mathbf{p}^{(i)2} \tag{7}$$

where the particle momenta are

$$\mathbf{p}^{(i)} = m^{(i)}\dot{\mathbf{c}}^{(i)} \tag{8}$$

with $\dot{\mathbf{c}}^{(i)}$ the velocity of the ith particle. The internal energy for the system is the sum

$$U = U_0 + U_1 + U_2 \tag{9}$$

where the first term represents the stored energy in the particles,

$$U_0 = \sum_{i=1}^{n} m^{(i)} u^{(i)}(\rho^{(i)}, s^{(i)}) \tag{10}$$

the second term represents stored energy due to hydrostatic tension in the subelements,

$$U_1 = \sum_{j=1}^{n_e} \sum_{k=1}^{6} \frac{1}{2}(1 - D^{(j)}) V_0^{(j,k)} \kappa_0^{(j)} (J^{(j,k)} - 1)^2 \, \Lambda(J^{(j,k)} - 1) \tag{11}$$

and the third term represents stored energy due to elastic shear in the hexahedra,

$$U_2 = \sum_{j=1}^{n_e} (1 - d^{(j)}) V_0^{(j)} \mu_0^{(j)} \, tr[\mathbf{E}^{e(j)T} \mathbf{E}^{e(j)}] \tag{12}$$

with $u^{(i)}$ the internal energy per unit mass for the particles, $\kappa_0^{(j)}$ and $\mu_0^{(j)}$ bulk and shear moduli for the elements, and $n_e$ the number of elements. The assumed internal energy function has the general form

$$U = U(\mathbf{c}^{(i)}, S^{(i)}, d^{(j)}, D^{(j)}, \mathbf{E}^{p(j)}) \tag{13}$$

and defines the generalized conservative forces

$$\mathbf{g}^{(i)} = \frac{\partial U}{\partial \mathbf{c}^{(i)}}, \qquad \theta^{(i)} = \frac{\partial U}{\partial S^{(i)}} \tag{14}$$

and the energy release rates

$$\mathbf{G}^{(j)} = -\frac{\partial U}{\partial \mathbf{E}^{p(j)}}, \qquad \Gamma^{d(j)} = -\frac{\partial U}{\partial d^{(j)}}, \qquad \Gamma^{D(j)} = -\frac{\partial U}{\partial D^{(j)}} \tag{15}$$

for the Hamiltonian model, where $\theta^{(i)}$ is the thermodynamic temperature. Having defined the stored energy for the system, the next section describes the dissipative process models.

## 7 Plasticity, damage, and viscosity models

Accurate hypervelocity impact models call for general descriptions of plastic flow, damage evolution, and material failure, and a numerical viscosity suitable for shock simulations. The plasticity model described here incorporates large strain kinematics, a rate dependent yield stress, and an isochoric plastic deformation constraint. The nonassociated flow rule is (Fahrenthold and Horban, 1997)

$$\dot{\mathbf{E}}^{p(j)} = \dot{\lambda}^{(j)} \{\frac{1}{2} tr[\mathbf{A}^{(j)T}\mathbf{A}^{(j)}]\}^{-1/2}\, \mathbf{A}^{(j)} \tag{16}$$

with

$$\mathbf{A}^{(j)} = \mathbf{C}^{p(j)}\mathbf{W}^{(j)} + \mathbf{W}^{(j)}\mathbf{C}^{p(j)} \tag{17}$$

where $\dot{\lambda}^{(j)}$ is a scalar multiplier and

$$\mathbf{W}^{(j)} = \mathbf{C}^{p(j)}\mathbf{S}^{(j)} + \mathbf{S}^{(j)}\mathbf{C}^{p(j)} - \frac{1}{3} tr[\mathbf{C}^{p(j)}\mathbf{S}^{(j)} + \mathbf{S}^{(j)}\mathbf{C}^{p(j)}]\, \mathbf{I} \tag{18}$$

with the deviatoric stress tensor and plastic Cauchy-Green strain tensor defined by

$$\mathbf{S}^{(j)} = (1 - d^{(j)})\, 2\, \mu_o^{(j)} \mathbf{E}^{e(j)}, \qquad \mathbf{C}^{p(j)} = \mathbf{I} + 2\, \mathbf{E}^{p(j)} \tag{19}$$

The assumed yield condition is

$$f^{(j)} = \tau^{(j)} - Y^{(j)}, \qquad \tau^{(j)} = \{\frac{1}{2} tr[\mathbf{S}^{(j)T}\mathbf{S}^{(j)}]\}^{1/2} \tag{20}$$

where $\tau^{(j)}$ is the effective stress. The yield stress $Y^{(j)}$ is

$$Y^{(j)} = (1 - d^{(j)})\{Y_0^{(j)}(1 + \beta_0^{(j)}\epsilon^{p(j)})^{n^{(j)}} + \beta_1^{(j)}\dot{\epsilon}^{(j)}\}\{1 - \beta_2^{(j)}\theta^{H(j)}\} \tag{21}$$

where $Y_0^{(j)}$ is the reference yield stress, $\epsilon^{p(j)}$ is the effective plastic strain, $\dot{\epsilon}^{(j)}$ is the effective strain rate, $\beta_0^{(j)}$ is a strain hardening modulus, $n^{(j)}$ is a strain hardening exponent, $\beta_1^{(j)}$ is a strain rate hardening modulus, $\beta_2^{(j)}$ is a thermal softening modulus, and $\theta^{H(j)}$ is the maximum historical homologous temperature. The yield stress is limited to a specified maximum value

$Y^{(j)}_{max}$. The plastic strain increment at each time step is determined using a one step iteration procedure with

$$\Delta\lambda^{(j)} = \frac{(\tau^{(j)} - Y^{(j)})\ \Lambda(\tau^{(j)} - Y^{(j)})}{(1 - d^{(j)})\ 2\ \mu_o^{(j)}} \tag{22}$$

The second dissipative process modeled is evolution of the continuum damage. The simplest forms increment the damage over a fixed number of time steps ($n_f$) once a failure criterion has been reached, for example

$$\Delta d^{(j)} = \frac{1}{n_f}\ max\{\ \Lambda(max[\sigma^{(j)}, t] - \sigma_{sp}^{(j)}),\ \Lambda(max[\epsilon^{p(j)}, t] - \epsilon_f^{(j)})\ \} \tag{23}$$

where $\sigma^{(j)}$ is the maximum eigenvalue of the deviatoric stress tensor, $\sigma_{sp}^{(j)}$ is a spall stress, $\epsilon_f^{(j)}$ is a failure strain, and the notation $max[X.t]$ denotes the maximum historical value of the argument $X$. Similarly for the normal damage

$$\Delta D^{(j)} = \frac{1}{n_f}\ \Lambda(max[P^{(j)}, t] - P^{c(j)}) \tag{24}$$

where $P^{(j)}$ is the average tensile pressure in the element and $P^{c(j)}$ is a critical pressure.

Alternately normal damage evolution may be calculated using the rate dependent form

$$\dot{D}^{(j)} = \frac{c_s^{(j)}}{h_p^{(j)}}\ \Lambda(P^{(j)} - P^{c(j)}) \tag{25}$$

where $c_s^{(j)}$ is the local soundspeed and $h_p^{(j)}$ is the local particle radius, or

$$\Delta D^{(j)} = (1 - D^{(j)})\ \frac{(P^{(j)} - P^{c(j)})}{P^{(j)}}\ \Lambda(P^{(j)} - P^{c(j)}) \tag{26}$$

where the damage increment at each time step serves to limit the tensile pressure, so as not to exceed the specified critical value.

Finally a numerical viscosity is introduced. A variety of numerical viscosity models are discussed in the literature (Noh, 1978). Most take the general form

$$\mathbf{f}^{(i)} = \sum_{j=1}^{n}\{C_0^{(i,j)}(\dot{\mathbf{c}}^{(i)} - \dot{\mathbf{c}}^{(j)}) + C_1^{(i,j)}|\dot{\mathbf{c}}^{(i)} - \dot{\mathbf{c}}^{(j)}|(\dot{\mathbf{c}}^{(i)} - \dot{\mathbf{c}}^{(j)})\} \tag{27}$$

where $C_0^{(i,j)}$ and $C_1^{(i,j)}$ are numerical viscosity coefficients, nonzero only for neighboring particles.

## 8 Entropy evolution

The entropy evolution equations take the general form

$$\dot{S}^{(i)} = \dot{S}^{irr(i)} - \dot{S}^{con(i)} \tag{28}$$

where the first term denotes irreversible entropy production due to the various dissipative processes and the second term is due to numerical heat conduction. These entropy evolution equations take the place of the energy balance relations included in conventional models of hypervelocity impact problems. The irreversible entropy production is calculated using

$$\theta^{(i)}\dot{S}^{irr(i)} = \mathbf{f}^{(i)} \cdot \dot{\mathbf{c}}^{(i)} + \sum_{k^{(i)}=1}^{n_e^{(i)}} \frac{1}{9} \{ \Gamma^{d(k^{(i)})}\dot{d}^{(k^{(i)})} + \Gamma^{D(k^{(i)})}\dot{D}^{(k^{(i)})} + tr[\mathbf{G}^{(k^{(i)})T}\dot{\mathbf{E}}^{p(k^{(i)})}] \} \tag{29}$$

where the $k^{(i)}$ are the element numbers associated with the ith particle, of number $n_e^{(i)}$. The entropy flow due to numerical conduction is quantified using

$$\theta^{(i)}\dot{S}^{con(i)} = \sum_{j=1}^{n} R^{(i,j)}(\theta^{(i)} - \theta^{(j)}) \tag{30}$$

where $R^{(i,j)}$ is a numerical conduction coefficient, nonzero only for neighboring particles.

## 9 Hamilton's equations

The final form of Hamilton's equations for the particle-element system may be derived using standard methods (Ginsberg, 1988), and consists of rate equations for the particle momentum and displacement states

$$\dot{\mathbf{p}}^{(i)} = -\mathbf{g}^{(i)} - \mathbf{f}^{(i)}, \qquad \dot{\mathbf{c}}^{(i)} = m^{(i)-1}\mathbf{p}^{(i)} \tag{31}$$

augmented by the evolution equations for the particle entropies and the element damage and plastic variables. These are explicit equations, which may be integrated using Runge-Kutta or other methods to solve the impact problem.

## 10 ISC projectile simulations

This section describes simulations of four different ISCL experiments, the latter performed by Grosch (1996 and 1997) on several different debris shield configurations. All of the simulations involved a projectile velocity of slightly over eleven kilometers per second, and all but one involved a velocity vector obliquity of 45 degrees. The ISCL projectiles were hollow aluminum cylinders with a length-to-diameter ratio less than two. and had a mass of approximately one gram. Since the projectile description was obtained from flash radiograph measurements, there is some uncertainty in the projectile mass and geometry data.

In general the ISC projectiles exhibited both pitch and yaw with respect to the velocity vector, hence all of the simulations reported here are fully three dimensional. The models were composed of 100,000-500,000 particles and required as much as four days to simulate 30-50 microseconds in physical time. The models were run in parallel on either 7 processors of an SGI Onyx or 32 processors of an SGI Origin, requiring up to 1GB of RAM. Computer resource constraints of course placed limits on the simulation times and the spatial resolutions of the models. Note that reducing the particle size by a factor of two would require a factor of eight increase in the number of particles and a factor of sixteen increase in the required wall clock time. Simulation parameters and material properties are listed in Appendices A and B.

The first simulation involved a 45 degree oblique impact on an aluminum Whipple shield at a standoff distance of 7.62 cm. Figures 1a and 1b show particle plots at impact and at 46.6 microseconds after impact, while Figure 1c shows an element plot of intact material at the simulation stop time. The simulation predicts a wall plate hole size (71 $\times$ 44 mm) somewhat greater than that observed in the experiment (60 $\times$ 20 mm).

The second simulation involved a 45 degree oblique impact on an aluminum Whipple shield at a standoff distance of 11.43 cm. Figures 2a and 2b show particle plots at impact and at 45.0 microseconds after impact, while Figure 2c shows an element plot of intact

material at the simulation stop time. The simulation predicts a perforated region in the wall plate (25 × 10 mm) similar in size to the hole observed in the experiment (20 × 15 mm).

The third simulation involved a normal impact on a dual plate aluminum shield at a standoff distance of 8.636 cm. In this case the axis of the cylindrical projectile and the velocity vector were significantly misaligned, again calling for a three dimensional simulation. Figures 3a and 3b show particle plots at impact and at 30.7 microseconds after impact, while Figure 3c shows an element plot of intact material at the simulation stop time. The simulation predicts a wall plate hole diameter (55 mm) somewhat greater than that observed in the experiment (44 mm).

The fourth simulation involved a 45 degree oblique impact on a multilayer aluminum-Nextel-Kevlar shield at a standoff distance of 7.62 cm. Figures 4a and 4b show particle plots at impact and at 46.2 microseconds after impact, while Figure 4c shows an element plot of intact material at the simulation stop time. Consistent with the experimental results, the simulation predicts bulging but not perforation of the wall plate. It should be noted that some relevant material properties of Nextel and Kevlar are not well known, and are currently under study (Hiermaier et al., 1999). Although the linear elastic response of many composite materials has been well characterized, information on thermomechanical equation of state properties and plasticity properties is incomplete. Although the latter information is normally of secondary interest in structural design calculations, it is certainly of major interest in hypervelocity impact applications.

The results just described indicate in general good agreement of the simulations with the experimental data. They do suggest a need for higher resolution models, longer physical simulation times, and better composite material models in future simulation work.

## 11 Projectile shape effect

As noted in the last section, the geometry of projectiles produced by ISCL experiments differs markedly from the solid spherical shape normally used in LGG tests. Since light

gas guns operate in a lower velocity regime, correlating the results of ISCL and LGG tests is complicated by an unknown projectile shape effect. In an attempt to investigate the significance of this projectile shape effect, the first three ISCL simulations described in the last section were repeated, with mass equivalent spherical projectiles replacing the actual hollow cylindrical ISC projectiles. Figures 5, 6, and 7 show element plots of the wall plate damage predictions obtained from simulations using hollow cylindrical ISCL projectiles and mass equivalent spherical projectiles, run in each case to the same simulation stop time.

The results suggest that ISCL projectiles are more damaging than mass equivalent spheres, although the magnitude of the difference is difficult to quantify. In the first and third cases the projectile mass exceeds significantly the ballistic limit mass, and in all cases higher resolution models of the impact problems are needed in order to draw more definitive conclusions. However it should be noted that since the ISC projectiles: (1) are hollow, (2) exhibit pitch and yaw with respect to their velocity vector, and (3) involve rather low length-to-diameter ratios, one might expect to observe a modest projectile shape effect. Considering the complex nature of these highly oblique hypervelocity impact problems, it appears that more experimental and computational work is needed to address the question of projectile shape effects.

## 12 Parallel speedup

Three dimensional impact simulations require large memory and CPU time allocations. Previous work on orbital debris shielding design (Faraud et al., 1999) has reported wall clock times as high as eighteen days for single processor simulations of three dimensional problems. Such turnaround times effectively preclude the use computer simulation in many engineering design projects. Parallel processing offers an opportunity to greatly reduce turnaround time and make three dimensional simulation a more practical design tool.

The code used in the present work (Fahrenthold, 1999) was written for parallel execution on Onyx and Origin systems, using loop level compiler directives based on the OpenMP

standard. Alternative parallel implementations based on MPI constructs are in general more portable and presumably more efficient, although more difficult to implement. It should be emphasized that a high degree of parallelism must be present in the basic numerical algorithm, in order to achieve good speedup under any coding scheme.

To evaluate parallel performance of the numerical algorithm and the code implementation used here, speedup tests were run on Origin systems with up to 128 processors. The test problems were large (300,000 - 500,000 particles), to insure that a meaningful load was maintained on each CPU as the processor allocation increased. Figure 8 shows the absolute speedup measured for a 500,000 particle test problem, based on the wall clock time required for ten time steps at various CPU allocations. The dotted line shows the maximum theoretical speedup, while the data points indicate the test results. At a CPU allocation of 64, the measured speedup is approximately two thirds of the theoretical maximum, indicating good parallel performance. At the maximum CPU allocation of 128, the efficiency drops to fifty percent. However the latter data point represents a factor of 64 reduction in wall clock time, indicating that a simulation which runs for over two months on one CPU can be run in one day on 128 processors.

Massively parallel systems are characterized by distributed memory architectures, complicating somewhat the practical interpretation of speedup test data. The Origin system discussed here is composed of a collection of compute *nodes*, each of which consists of two processors and 512 MB of RAM. An individual user is allocated a discrete number of nodes for each particular job, that is allocations consisting of arbitrary combinations of processors and RAM are not permitted. As a result, a job which requires 1 GB of RAM will be allocated a minimum of four processors, and the meaningful speedup curve for such a problem is one measured relative to a CPU allocation of four. Figure 9 shows the results of a relative speedup test run on an Origin system, for ten time steps of a 300,000 particle test problem, using the code discussed in the present work. The solid line represents the maximum theoretical relative speedup, while the data points show the test results. Again the data shows

good speedup for processor allocations as high as 64.

High performance parallel computer systems are not yet commonplace in engineering design work. However the preceding results demonstrate that the numerical method used here can effectively exploit such resources, an important consideration as low cost, high performance parallel hardware becomes more widely available.

## 13 Conclusion

The present report describes a systematic test of the use of parallel computation and a hybrid particle-element algorithm to simulate a range of three dimensional orbital debris impact experiments. The numerical method appears to offer certain advantages in addressing the three dimensional, multi-plate shield design problem. Additional work is needed to investigate model resolution, simulation time, projectile shape, and material property effects (including for example the use of the SESAME equation of state models). However developments to date suggest that massively parallel computation using some type of mixed particle-continuum scheme offers excellent opportunities for significant advances in simulation-based debris shield design.

## 14 Acknowledgements

This work was supported by the Hypervelocity Impact Technology Facility, Space Science Branch, NASA Johnson Space Center. Computer time support was provided by the Numerical Aerospace Simulation facility at NASA Ames Research Center and the Texas Advanced Computing Center.

## 15 References


Baumeister, T., editor, 1978, MARK'S STANDARD HANDBOOK FOR MECHANICAL ENGINEERS, McGraw-Hill, New York.

Belytschko, T., Krongauz, Y., Organ, D., Fleming, M., and Krysl, P., 1996, "Meshless Methods: An Overview and Recent Developments," *Computer Methods in Applied Mechanics and Engineering*, Vol. 139, pp. 3-47.

Budge, K.G. and Peery, J.S., 1993, "RHALE: A MMALE Shock Physics Code Written in C++," *International Journal of Impact Engineering*, Vol. 14, pp. 107-120.

Christiansen, E.L., Kerr, J.H., de la Fuente, H.M., and Schneider, W.C., 1999, "Flexible and Deployable Meteoroid/Debris Shielding for Spacecraft," *International Journal of Impact Engineering*, Vol. 23, pp. 125-136.

Fahrenthold, E.P., 1998, "Numerical Simulation of Impact on Hypervelocity Shielding," PROCEEDINGS OF THE HYPERVELOCITY SHIELDING WORKSHOP, Galveston, Texas, pp. 47-50.

Fahrenthold, E.P., 1999, USER'S GUIDE FOR EXOS, University of Texas, Austin.

Fahrenthold, E.P., and Horban, B.A., 1997, "Thermodynamics of continuum damage and fragmentation models for hypervelocity impact," *International Journal of Impact Engineering*, Vol. 20, pp. 241-252.

Fahrenthold, E.P., and Horban, B.A., 1999, "A Hybrid Particle-Finite Element Method for Hypervelocity Impact Simulation," *International Journal of Impact Engineering*, Vol. 23, pp. 237-248.

Fahrenthold, E.P., and Horban, B.A., 2000, "An Improved Hybrid Particle-Element Method for Hypervelocity Impact Simulation," submitted for presentation at the 2000 Hypervelocity Impact Symposium.

Fahrenthold, E.P., and Koo, J.C., 2000, "Hybrid Particle-Element Bond Graphs for Impact Dynamics Simulation," *Journal of Dynamic Systems, Measurement, and Control*, in

press.

Faraud, M., Destefanis, R., Palmieri, D., and Marchetti, M., 1999, "SPH Simulations of Debris Impacts Using Two Different Computer Codes," *International Journal of Impact Engineering*, Vol. 23, pp. 249-260.

Ginsberg, J.H., 1988, ADVANCED ENGINEERING DYNAMICS, Harper and Row, Inc., Cambridge.

Grady, D., 1999, "Impact Failure and Fragmentation Properties of Tungsten Carbide," *International Journal of Impact Engineering*, Vol. 23, pp. 307-317.

Grosch, D.J., 1996, INHIBITED SHAPED CHARGE LAUNCHER TESTING OF SPACECRAFT SHIELD DESIGNS, Southwest Research Institute, San Antonio, Texas.

Grosch, D.J., 1997, INHIBITED SHAPED CHARGE LAUNCHER TESTING OF SPACECRAFT SHIELD DESIGNS, Southwest Research Institute, San Antonio, Texas.

Hallquist, J.O., 1983, THEORETICAL MANUAL FOR DYNA3D, Lawrence Livermore National Laboratory, Livermore, California.

Hayhurst C.J., Livingstone, I.H., Clegg, R.A., Fairlie, G.E., Hiermaier, S.H., and Lambert, M., 1998, "Numerical Simulation of Hypervelocity Impacts on Aluminum and Nextel/Kevlar Whipple Shields," PROCEEDINGS OF THE HYPERVELOCITY SHIELDING WORKSHOP, Galveston, Texas, pp. 61-72.

Hiermaier, S., Riedel, W., Hayhurst, C.J., Clegg, R.A., and Wentzel, C.M., 1999, ADVANCED MATERIAL MODELS FOR HYPERVELOCITY IMPACT SIMULATIONS, EMI-Report Number E 43/99, Freiburg, Germany.

Johnson, G.R., Petersen, E.H., and Stryk, R.A., 1993, "Incorporation of an SPH option into the EPIC code for a wide range of high velocity impact computations," *International Journal of Impact Engineering*, Vol. 14, pp. 385-394.

Lee, S.L., editor, 1989, REFERENCE BOOK FOR COMPOSITES TECHNOLOGY, Technomic Publishing, Lancaster, Pennsylvania.

Libersky, L.D., Randles, P.W., Carney, T.C., and Dickinson, D.L., 1997, "Recent Im-

provements in SPH Modeling of Hypervelocity Impact," *International Journal of Impact Engineering*, Vol. 20, pp. 525-532.

Liu, W.K., Hao, S., Belytschko, T., Li, S., and Chang, C.T., 2000, "Multi-scale Methods," *International Journal for Numerical Methods in Engineering*, Vol. 47, pp. 1343-1361.

McGlaun, J.M., Thompson, S.L., and Elrick, M.G., 1990, "CTH: A Three Dimensional Shock Wave Physics Code," *International Journal of Impact Engineering*, Vol. 10, pp. 351-360.

Noh, W.F., 1978, "Errors for Calculations of Strong Shocks Using an Artificial Viscosity and an Artificial Heat Flux," *Journal of Computational Physics*, Vol. 72, pp. 78-120.

Steinberg, D.J., 1996,EQUATION OF STATE AND STRENGTH PROPERTIES OF SELECTED MATERIALS, Lawrence Livermore National Laboratory, UCRL-MA-106439.

Stellingwerf, R.F., and Wingate, C.A., 1993, "Impact Modeling with Smooth Particle Hydrodynamics," *International Journal of Impact Engineering*, Vol. 14, pp. 707-718.

# A Appendix: simulation parameters

The simulated experiments are described in detail by Grosch (1996 and 1997).

| Simulation parameters | | | | |
|---|---|---|---|---|
| Parameter | Case 1 | Case 2 | Case 3 | Case 4 |
| SWRI Test Number | 7139-19 | 7139-22 | 7139-03 | 7139-24 |
| Shield type | Al Whipple | Al Whipple | Al dual plate | Al-composite |
| First aluminum plate thickness (cm) | 0.127 | 0.127 | 0.16002 | 0.127 |
| Second aluminum plate thickness (cm) | 0.0 | 0.0 | 0.3175 | 0.0 |
| Nextel areal density ($g/cm^2$) | 0.0 | 0.0 | 0.0 | 0.4 |
| Kevlar areal density ($g/cm^2$) | 0.0 | 0.0 | 0.0 | 0.128 |
| Wall plate thickness (aluminum, cm) | 0.4826 | 0.4826 | 0.2032 | 0.3175 |
| Maximum standoff (cm) | 7.62 | 11.43 | 8.636 | 7.62 |
| Impact velocity (km/sec) | 11.41 | 11.30 | 11.16 | 11.25 |
| Impact obliquity (velocity vector, deg) | 45 | 45 | 0 | 45 |
| Projectile mass (aluminum, g) | 1.38 | 0.85 | 1.30 | 1.07 |
| Projectile length-to-diameter ratio | 1.4 | 1.2 | 1.84 | 1.1 |
| Projectile pitch (wrt velocity vector, deg) | 0 | 11.6 | 12.6 | 0 |
| Projectile yaw (wrt velocity vector, deg) | 9.4 | 19.3 | 6.9 | 0 |
| Number of particles | 142,867 | 305,551 | 265,251 | 415,413 |
| Simulation time ($\mu$sec) | 46.6 | 45.0 | 30.7 | 46.2 |
| Wall clock time (hours) | 28.1 | 15.6 | 15.6 | 109.3 |
| Average number of processors | 6.9 | 32 | 32 | 7.3 |
| System | Onyx | Origin | Origin | Onyx |

# B Appendix: material properties

Material properties were estimated using data from Steinberg (1996), Lee (1989), and Hiermaier et al. (1999). As indicated in the text, material models for the composites are the subject of current research. Listed below are the material properties used in the simulations.

| Material properties | | | |
|---|---|---|---|
| Parameter | Aluminum | Nextel | Kevlar |
| Equation of state type | Mie-Gruneisen | Linear | Linear |
| Shear modulus (Mbar) | 0.271 | 0.164 | 0.100 |
| Reference bulk density (g/cc) | 2.7 | 0.82021 | 0.741084 |
| Reference bulk modulus (Mbar) | 0.7832 | 0.66633 | 0.415389 |
| Initial yield stress (Mbar) | 0.0029 | 0.008 | 0.008 |
| Maximum yield stress (Mbar) | 0.0058 | 0.008 | 0.008 |
| Strain hardening exponent | 0.1 | 0 | 0 |
| Strain hardening modulus | 125.0 | 0 | 0 |
| Thermal softening modulus | 0.5 | 1.0 | 1.0 |
| Melt temperature (kilodegrees Kelvin) | 1.22 | 1.22 | 0.70 |
| Specific heat (Mbar-$cm^3$ per g-kilodegrees Kelvin) | $0.884 \times 10^{-2}$ | $0.884 \times 10^{-2}$ | $1.420 \times 10^{-2}$ |
| Spall stress (Mbar) | 0.012 | 0.100 | 0.100 |
| Plastic failure strain | 2.0 | 0.2 | 0.2 |

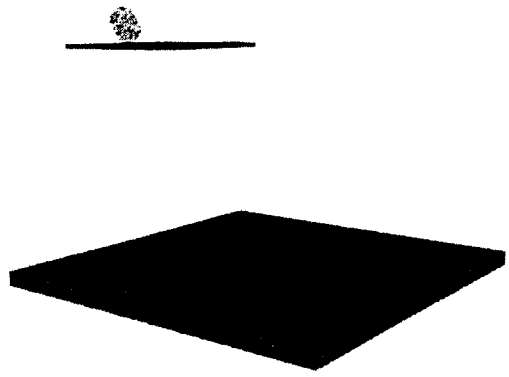

Figure 1a. Whipple shield with 7.62 cm standoff.

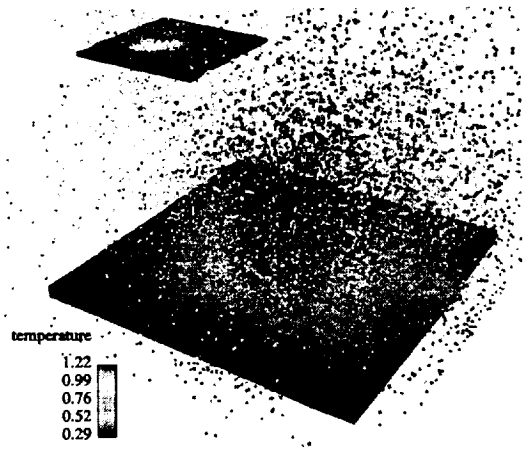


Figure 1b. Particle plot at t = 46.6 microseconds.

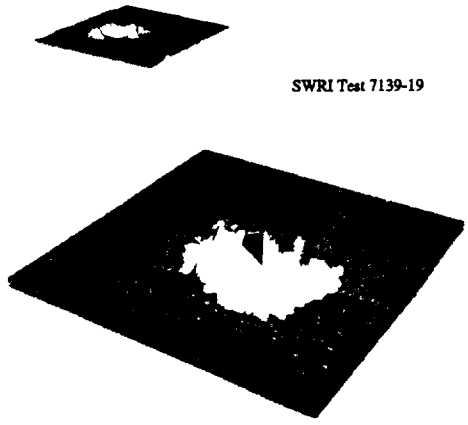


Figure 1c. Element plot at t = 46.6 microseconds.

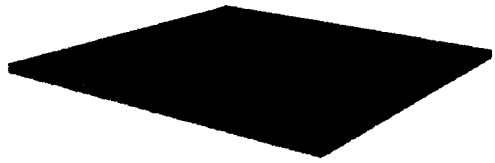

Figure 2a. Whipple shield with 11.43 cm standoff.

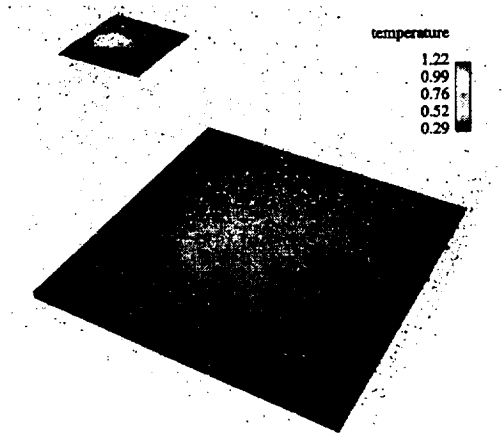


Figure 2b. Particle plot at t = 45.0 microseconds.

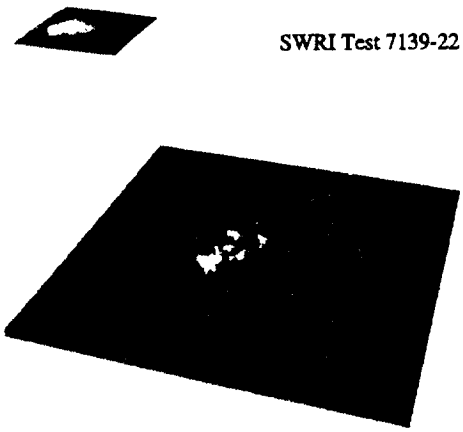


Figure 2c. Element plot at t = 45.0 microseconds.

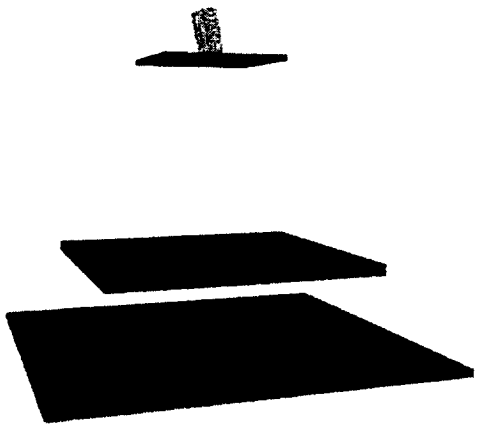

Figure 3a. Aluminum dual plate shield.

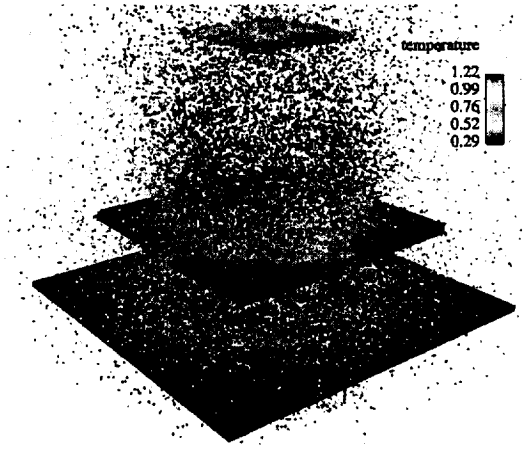


Figure 3b. Particle plot at t = 30.7 microseconds.

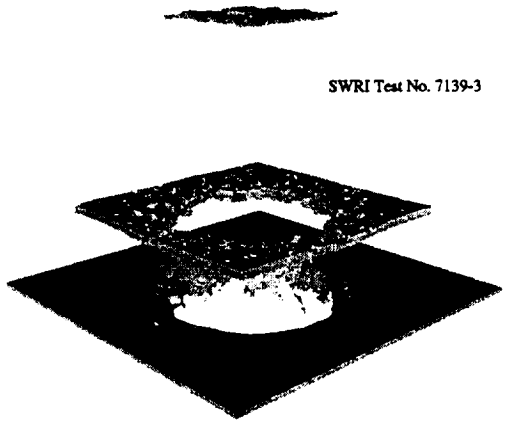


Figure 3c. Element plot at t = 30.7 microseconds.

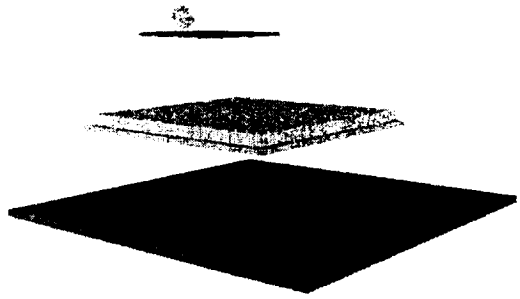

Figure 4a. Aluminum-Nextel-Kevlar shield.

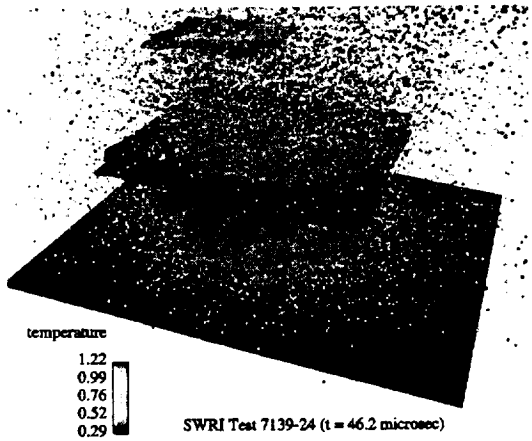


Figure 4b. Particle plot at t = 46.2 microseconds.

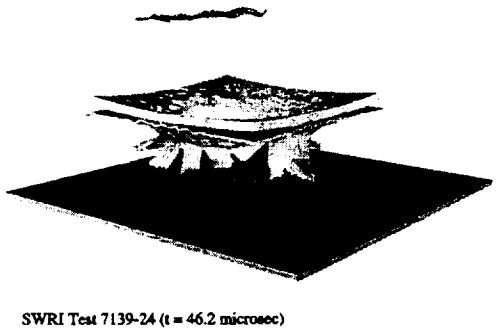


Figure 4c. Element plot at t = 46.2 microseconds.

Figure 5a. Wall damage for ISC projectile,
Whipple shield with 7.62 cm standoff.

Figure 5b. Wall damage for spherical projectile,
Whipple shield with 7.62 cm standoff.

Figure 6a. Wall damage for ISC projectile,
Whipple shield with 11.43 cm standoff.

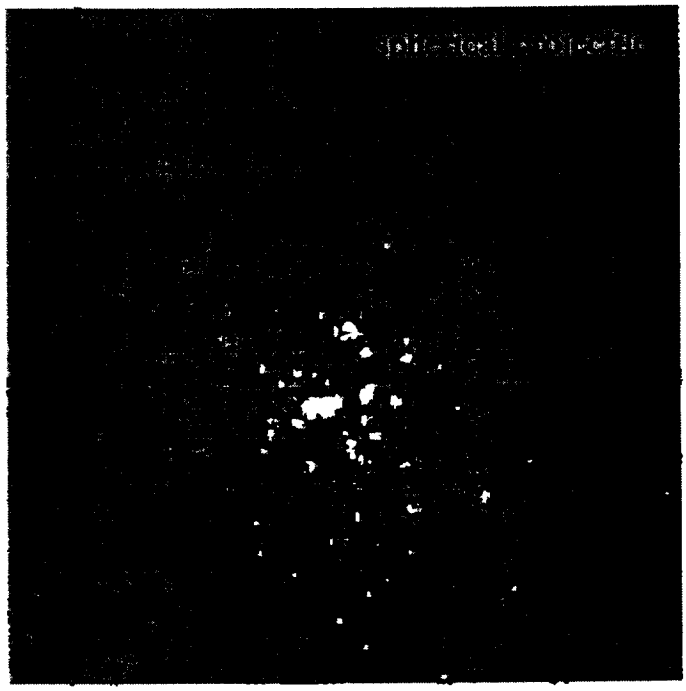

Figure 6b. Wall damage for spherical projectile,
Whipple shield with 11.43 cm standoff.

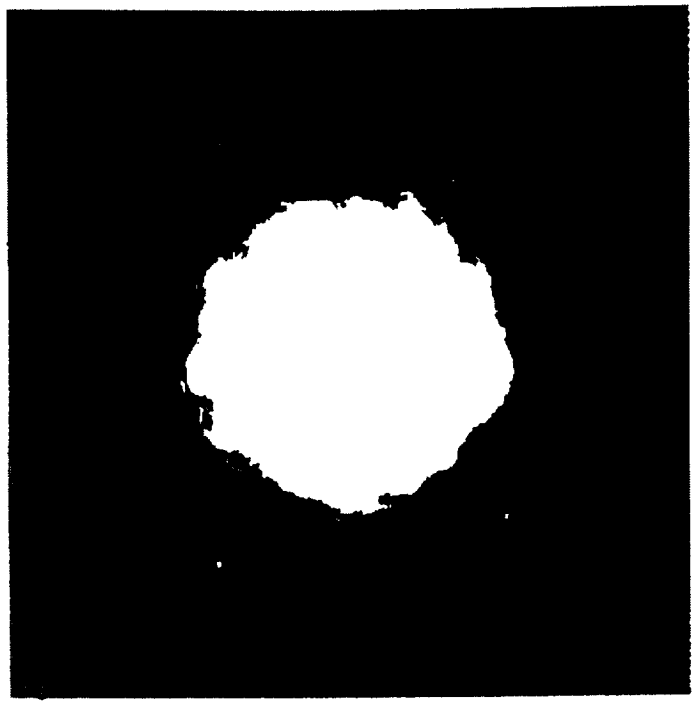

Figure 7a. Wall damage for ISC projectile,
dual plate aluminum shield.

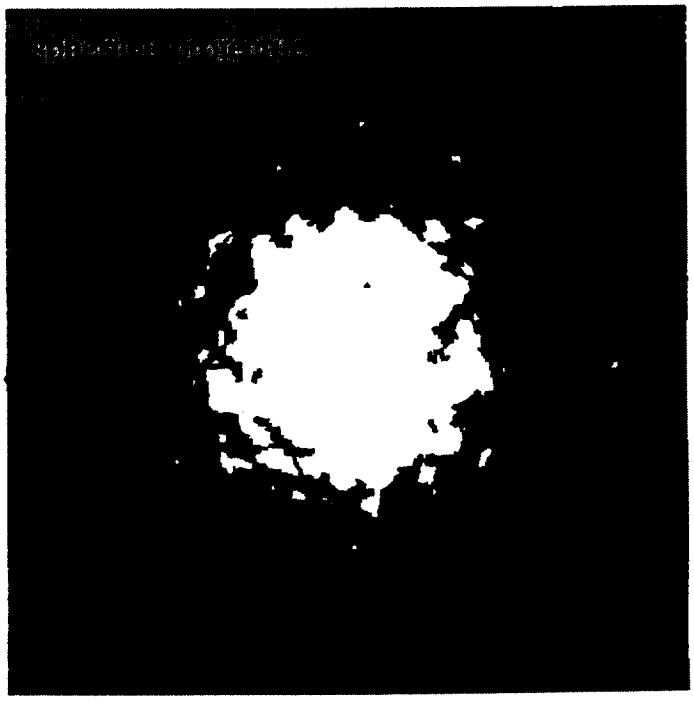

Figure 7b. Wall damage for spherical projectile,
dual plate aluminum shield.

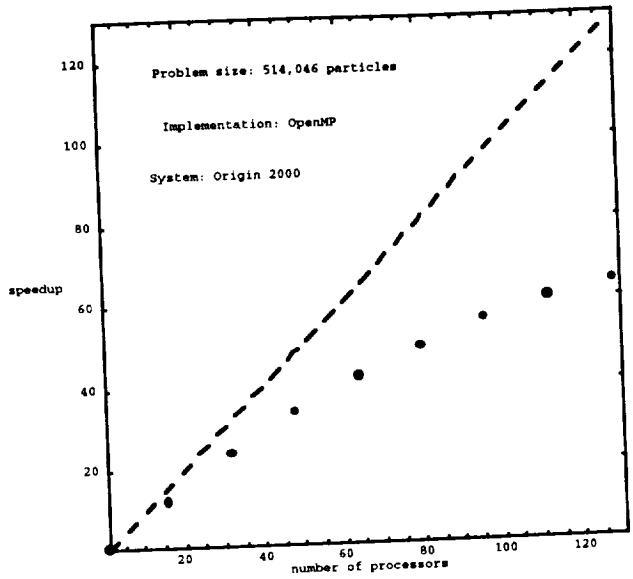


Figure 8. Absolute speedup for a problem with 500,000 particles.

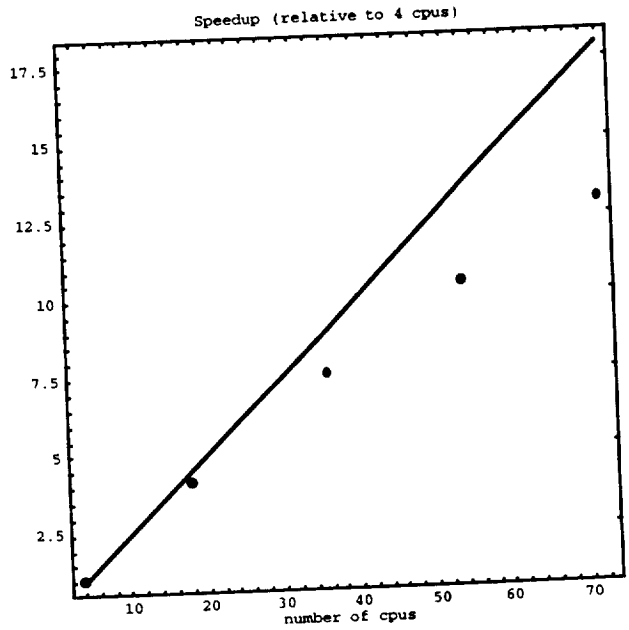


Figure 9. Relative speedup for a problem with 300,000 particles.